European Journal of Radiology 116 (2019) 76–83

Contents lists available at ScienceDirect

European Journal of Radiology

journal homepage: www.elsevier.com/locate/ejrad

Research article

Automated plaque analysis for the prognostication of major adverse cardiac events

Marly van Assen[a,b], Akos Varga-Szemes[a], U. Joseph Schoepf[a,*], Taylor M. Duguay[a], H. Todd Hudson[a], Svetlana Egorova[c], Kjell Johnson[d], Samantha St. Pierre[c], Beatrice Zaki[a], Matthijs Oudkerk[b], Rozemarijn Vliegenthart[a,b,e], Andrew J. Buckler[c]

[a] Division of Cardiovascular Imaging, Department of Radiology and Radiological Science, Medical University of South Carolina, Charleston, SC, USA
[b] University of Groningen, University Medical Center Groningen, Center for Medical Imaging, Groningen, the Netherlands
[c] Elucid Bioimaging Inc., Wenham, MA, USA
[d] Stat Tenacity, Ann Arbor, MI, USA
[e] University of Groningen, University Medical Center Groningen, Department of Radiology, Groningen, the Netherlands

ARTICLE INFO

Keywords:
Plaque analysis
Automated analysis
Computed tomography
MACE
Prognostication
Coronary artery disease

ABSTRACT

Objective: The purpose of this study is to assess the value of an automated model-based plaque characterization tool for the prediction of major adverse cardiac events (MACE).
Methods: We retrospectively included 45 patients with suspected coronary artery disease of which 16 (33%) experienced MACE within 12 months. Commercially available plaque quantification software was used to automatically extract quantitative plaque morphology: lumen area, wall area, stenosis percentage, wall thickness, plaque burden, remodeling ratio, calcified area, lipid rich necrotic core (LRNC) area and matrix area. The measurements were performed at all cross sections, spaced at 0.5 mm, based on fully 3D segmentations of lumen, wall, and each tissue type. Discriminatory power of these markers and traditional risk factors for predicting MACE were assessed.
Results: Regression analysis using clinical risk factors only resulted in a prognostic accuracy of 63% with a corresponding area under the curve (AUC) of 0.587. Based on our plaque morphology analysis, minimal cap thickness, lesion length, LRNC volume, maximal wall area/thickness, the remodeling ratio, and the calcium volume were included into our prognostic model as parameters. The use of morphologic features alone resulted in an increased accuracy of 77% with an AUC of 0.94. Combining both clinical risk factors and morphological features in a multivariate logistic regression analysis increased the accuracy to 87% with a similar AUC of 0.924.
Conclusion: An automated model based algorithm to evaluate CCTA-derived plaque features and quantify morphological features of atherosclerotic plaque increases the ability for MACE prognostication significantly compared to the use of clinical risk factors alone.

1. Introduction

Coronary computed tomography angiography (CCTA) has been increasingly used for the evaluation of coronary artery disease (CAD). Its high negative predictive value makes CCTA especially suitable for ruling out CAD [1,2]. Additionally, CCTA enables non-invasive atherosclerotic plaque evaluation which can be used for diagnostic and prognostic purposes [3,4].

Abbreviations: AUC, area under the curve; CABG, coronary artery bypass grafting; CAD, coronary artery disease; CALC, calcified plaque volume; CCTA, coronary computed tomography angiography; CNR, contrast to noise ratio; DSCT, dual source CT; LAD, left anterior descending artery; LCx, left circumflex artery; LRNC, lipid rich necrotic core; MACE, major adverse cardiac events; MATX, matrix/fibrous tissue volume; MI, myocardial infarction; PCI, percutaneous coronary intervention; RCA, right coronary artery; ROC, receiver operating characteristic; SIS, segment involvement score; SNR, signal to noise ratio; SSS, segment stenosis score; wSD, within section standard deviation

* Corresponding author at: Department of Radiology and Radiological Science, Medical University of South Carolina, 25 Courtenay Drive, Charleston, SC, USA.
E-mail addresses: vanasse@musc.edu (M. van Assen), vargaasz@musc.edu (A. Varga-Szemes), schoepf@musc.edu, griffile@musc.edu (U.J. Schoepf), duguay@musc.edu (T.M. Duguay), hudsonhe@musc.edu (H.T. Hudson), svetlana.egorova@elucidbio.com (S. Egorova), kjell@stattenacity.com (K. Johnson), samantha.stpierre@elucidbio.com (S. St. Pierre), zaki@musc.edu (B. Zaki), m.oudkerk@rug.nl (M. Oudkerk), r.vliegenthart@umcg.nl (R. Vliegenthart), andrew.buckler@elucidbio.com (A.J. Buckler).

https://doi.org/10.1016/j.ejrad.2019.04.013
Received 31 January 2019; Received in revised form 26 March 2019; Accepted 21 April 2019
0720-048X/ Published by Elsevier B.V.

Several CT-based risk scores such as the traditional Agatston calcium score, the segment involvement score (SIS), and segment stenosis score (SSS) have demonstrated improved predictive value for future cardiac events compared to clinical risk factors [5–7]. Furthermore, previous studies have proposed that morphological and functional plaque characteristics, such as plaque burden and composition, can aid in the prognostication of major adverse cardiac events (MACE) [8–10]. Patients with non-obstructive CAD and a high-risk plaque profile based on CCTA analysis can be assigned to the most appropriate therapy and/or longitudinal follow-up for possible intensification or downgrading of therapy [3,10].

For CCTA to enter the mainstream of diagnostic clinical care, it is necessary to decrease observer variability and automate key parts of the interpretive process to manage the subjectivity, time-consuming nature, and variability of reader interpretation. Key candidates for automation are those tasks that are the most challenging for human readers, such as resolving key interfaces despite partial volume effects, calcium blooming, overlapping HU ranges, and providing objective quantitation of plaque burden and characterization.

The purpose of this study is to assess the value of an automated model-based plaque characterization tool for the prediction of MACE.

2. Materials and methods

2.1. Patients

The study protocol was approved by the institutional review board and a waiver of informed consent was granted. We retrospectively included patients with suspected CAD from a previously described cohort [11]. A total of 92 patients with suspected CAD from two centers in the US and Europe who had undergone CCTA with a follow-up of 12 months were included. For the current study, only patients from one center were included, leaving 48 patients for analysis of which 16 (33%) experienced MACE within 12 months. The previous study focused on manually deriving quantitative information on coronary plaque burden whereas the current study used a semi-automated method to analyze coronary plaque using a non-threshold based approach. All patients had undergone CCTA for clinical indications between January 2006 and September 2014 and had a follow-up period of 12 months for MACE. Patients were excluded if they were diagnosed with acute coronary syndrome during the episode of care involving the CCTA scan, underwent coronary revascularization within 30 days of the CT scan, or had a history of myocardial infarction (MI), percutaneous coronary intervention (PCI) or coronary artery bypass grafting (CABG). Additionally, CCTA data with non-diagnostic image quality were excluded.

2.2. Clinical data

MACE were defined as death due to cardiac causes, non-fatal MI, or unstable angina leading to coronary revascularization (PCI or CABG) more than 30 days after CCTA. For each patient, the date of each MACE was recorded. In the case of no MACE, the date of last known follow up was recorded. Relevant clinical data and risk factors were collected from medical records. This included but was not limited to: patient history/ demographics, medications, risk factors, and patient management. Risk factors were articulated in terms of the Framingham Risk Score and its components.

2.3. Imaging protocols

Sixty-four-slice CT, 1st, 2nd, and 3rd generation dual-source CT (DSCT) systems (Somatom AS+, Somatom Definition, Somatom Definition Flash, Somatom Force, Siemens Healthineers, Forchheim, Germany) were used for CCTA acquisitions. All patients initially underwent a non-contrast enhanced calcium scoring scan (120 kV tube voltage; tube current, 75 mA; 3-mm slice thickness with 1.5 mm increment). For the subsequent contrast-enhanced coronary CTA, scan parameters were as follows: a retrospectively ECG-gated protocol for the 64-slice CT and 1 st generation DSCT scanners, and a prospectively ECG-triggered sequential scan protocol for the 2nd and 3rd generation DSCT scanners (tube voltage of 100–120 kV, tube current of 700–800 mA for the 64-slice CT, and 320–412 mA for 1st-3rd generation DSCT). For the CCTA, contrast enhancement was achieved by injecting 50–80 mL iopromide (Ultravist 370mgI/mL, Bayer, Wayne, NJ) at 4–6 mL/s followed by a 30 ml saline bolus chaser. Beta-blockers and nitroglycerine were used if necessary at the discretion of the attending physician. Image reconstruction was performed at the optimal cardiac phase with a section thickness of 0.75 mm, a reconstruction increment of 0.5 mm, and a smooth convolution kernel.

2.4. Image analysis

Image quality of each scan was rated on a 5-point Likert-scale (1-poor image quality, 5 excellent image quality), signal-to-noise ratio (SNR), and contrast-to-noise ratio (CNR). SNR was calculated as the HU value in the myocardium divided by the SD of the HU in the myocardium. The CNR was calculated as the difference in Hu values between the myocardium and cardiac fat divided by the SD of cardiac fat.The HU values and SDs were measured by placing ROI in the myocardium and in the cardiac fat areas. All image quality measurements, subjective and objective, were performed by a physician with 3 years experienced in cardiac imaging.

Vessel sharpness of the left anterior descending (LAD) and right coronary arteries (RCA) were also calculated. All scans with poor image quality were excluded from further analysis.

Subsequently, commercially available plaque quantification software (vascuCAP, Elucid Bioimaging, Wenham, MA) (see Supplement for performance validation) was used to extract quantitative plaque morphology. Lesions were marked manually based on the software's plaque morphology assessment. Cap thickness was measured by the user based on the software determined 3D LRNC region(s). All measurements were performed by a physician with 3 years experienced in cardiac imaging and were validated by an experienced cardiac radiologist (+years of experience). The measurements were performed at all cross sections, spaced at 0.5 mm, based on fully 3D segmentations of lumen, wall, and each tissue type. Absolute volume per target and per lesion, cross-sectional area for each cross section at .5 mm spacing, proportional occupancy of each, and maximum cross-sectional area and proportion for each target and lesion are calculated. Wall area or volume is calculated as the overall vessel volume or area minus the lumen area or volume. Plaque burden was assessed as the ratio of wall area or volume divided by the overall vessel area or volume. Lesion length was calculated using the centerline in 3D. All volume calculations are determined from 3D regions at the overall target as well as marked lesion levels. Vessel structure measurements included the degree of stenosis (calculated both by area or diameter), wall thickness (distance between the lumen boundary to outer vessel wall boundary), and remodeling ratio (the ratio of vessel area with plaque to a vessel area without plaque). Measurements for tissue characteristics included calcified plaque volume (CALC) with the largest cross-sectional area and proportion, lipid-rich necrotic core plaque volume (LRNC) with the largest cross-sectional area and proportion, and matrix/fibrous tissue volume (MATX) with the largest cross-sectional area and proportion (see the Supplement for formal definitions for the tissue types).

Analyses were performed within the proximal and mid segments of the three major coronary arteries (LAD, LCX and RCA) using the semi-automated plaque analysis algorithm.

The algorithm, with user input, generated a centerline through the lumen of each vessel. The longitudinal boundaries for the vessels were set from the origin to a point where the vessel diameter is less than 2 mm. Cross-sectional spatial boundaries were adjusted to include the

Table 1
Scanner technology effects on image quality.

	Siemens AS+	Siemens Definition	Siemens Flash	Siemens Force	p
Image quality rating	4.0 [3.5; 4.5]	4.5 [4.0; 5.0]	4.0 [4.0; 5.0]	4.5 [4.0; 5.0]	0.577
SNR – LAD	23.7 ± 7.9	23.6 ± 8.6	18.5 ± 10.5	25.3 ± 15.5	0.755
SNR – RCA	22.1 ± 6.5	23.9 ± 9.1	17.6 ± 10.4	27.5 ± 17.0	0.584
CNR – LAD	21.8 ± 7.3	21.6 ± 8.2	17.8 ± 10..0	23.9 ± 14.8	0.755
CNR – RCA	21.1 ± 5.9	22.0 ± 8.7	17.0 ± 9.7	16.1 ± 16.4	0.564
Sharpness – LAD	51.1 ± 4.0	54.1 ± 4.6	52.4 ± 6.5	59.1 ± 6.0	0.173
Sharpness – RCA	54.4 ± 3.9	56.7 ± 7.0	54.4 ± 6.1	57.5 ± 7.0	0.332

full thickness of the vessel wall while minimizing the inclusion of surrounding tissue such as myocardium and fat. Window levels could be adjusted manually to exclude, for example, blooming effects from calcifications.

The software used a novel method for the classification of composition of vascular plaque components that was validated on expert-annotated histology with *ex vivo* to in vivo image registration, independent of the vascuCAP outputs [12]. The multi-scale model computes the statistics of each contiguous region of a given analyte type. Each plaque region is labeled by analyte type, and various position/shape descriptors are computed. Within each plaque region, each voxel can produce a radiological imaging intensity value, which are modeled as independent and identically distributed samples that come from a continuously valued distribution specific to each analyte type. One key feature of this model is that it accounts for the spatial relationship of analytes within the vessel and also to each other, recognizing that point-wise image intensity (whether from histology and/or imaging) is not the only source of information used by experts to determine plaque composition. The software corrects the HU values for the partial volume effect, often experienced as blooming artifacts from calcified plaque and enhanced arterial lumen as well as reduced ability to discriminate LRNC. Subsequently, the software applies an iterative optimization algorithm informed, but not constrained, by partially overlapping HU ranges for different tissue types.

To address imaging artifacts caused by calcified plaque and enhanced arterial lumen, which hinders the accuracy of sub-voxel measurements, the software determines the patient-specific imaging system point spread function with an algorithm that probabilistically estimates the most likely fine structure, given the magnitude of image blur. This image-based determination of blur, coupled with sub-voxel analysis of plaque component densities, leads to more accurate scoring of coronary artery calcification. This allows the quantification of subtle changes in LRNC and consequently, cap thickness. The accuracy of tissue characteristic measurements has been previously validated by histology with measurement bias recorded at -0.096, 1.26, and -2.44 mm^2 for CALC, LRNC, and MATX respectively [12].

To assess intra-observer repeatability, the same observer performed the same measurements for fourteen randomly selected patients after a 3-week period from the observer's last read. To assess inter-observer reproducibility, a second observer performed the measurements for these selected patients.

2.5. Statistical analysis

To address whether different scanner generations may affect analysis, we conducted an evaluation of the image quality between scanners on all patients. Univariate and multivariate logistic regression models were used to analyze the prognostic value of clinical risk factors, morphological features, and both combined. Recursive feature elimination was used to select features using 5 repeats of 10-fold cross-validation for each predictor set to find the optimal subset of predictors and to estimate the predictive model performance using receiver operating characteristic (ROC), while protecting against overfitting. Therefore, the predictors that are selected are appropriate for predicting new, yet-to-be-seen data. The software was locked down after each of the two readers processed the five training cases selected at random. The predictive accuracy of the final model in regards to MACE was calculated, including the area under the curve (AUC), sensitivity, specificity, as well as the measurement variability (intra- and inter-reader) associated with the software measurements. For each measurement, we calculated the within-section Standard Deviation (wSD) estimated from two replicate calculations by the same reader (intra-reader) and by two different readers (inter-reader). Measurements analyzed were lumen area, wall area, stenosis percentage, wall thickness, calcified area, LRNC area, matrix area and plaque burden (see supplement for descriptions). 95%-CIs were determined using a chi square statistic as the pivotal statistic. Also in this study, manual measurements by on-screen calipers were made for stenosis and wall thickness.

3. Results

A total of 45 patients (59 ± 8.5 years, 71% male) with suspected CAD and similar risk profile who had undergone CCTA were analyzed. Three patients were excluded due to poor image quality. Of these 45 patients, 16 (33%) experienced MACE within 12 months.

3.1. Image quality

All patients were analyzed for image quality, subjectively and objectively. No significant differences in image quality related parameters among the four different scanner types were observed, Table 1.

Table 2
Reader variability for semi-automated measurements.

Structure	Lumen Area, range 1.5-37.2 mm^2	*Inter-reader wSD*: 3.0mm^2 [2.6, 3.4], *Intra-reader wSD*: 1.8mm^2 [1.6, 2.1]
	Wall Area, range 3.5-40.6mm^2	*Inter-reader wSD*: 2.9mm^2 [2.6, 3.5], *Intra-reader wSD*: 1.8mm^2 [1.6, 2.1]
	Stenosis, range 1.9-80.4%	*Inter-reader wSD*: 9.3% [7.8, 11.6], *Intra-reader wSD*: 8.6% [7.1, 8.9]
	Wall Thickness, range 1.1-3.8mm	*Inter-reader wSD*: 0.3 mm [0.3, 0.4], *Intra-reader wSD*: 0.2 mm [0.2, 0.3]
Composition	Calcified Area, range 0.0-12.4mm^2	*Inter-reader wSD*: 0.7mm^2 [0.6, 0.8], *Intra-reader wSD*: 0. 6mm^2 [0.6, 0.8]
	LRNC Area, range 0.0-7.6mm^2	*Inter-reader wSD*: 0.6mm^2 [0.5, 0.7], *Intra-reader wSD*: 0.5 mm^2 [0.4, 0.6]
	Matrix Area, range 3.1-32.1mm^2	*Inter-reader wSD*: 2.3 mm^2 [2.1, 2.7], *Intra-reader wSD*: 1.4mm^2 [1.3, 1.6]
	Plaque Burden, range 0.3-0.9 (ratio)	*Inter-reader wSD*: 0.05 [0.04, 0.05], *Intra-reader wSD*: 0.05 [0.04, 0.06]

Table 3
Risk factor summary statistics.

Risk Factor	MACE – (n = 29)	MACE + (n = 16)	p-value
Binary risk factors			
Sex	76% (22)	62% (10)	0.5
Race	31% (9)	50% (8)	0.3
Hypercholesterlemia	41% (12)	62% (10)	0.2
Type 2 Diabetes	21% (6)	31% (5)	0.5
Hypertension	66% (19)	62% (10)	1.000
Continuous risk factors			
Age	58.6 + /-0.3	59.8 + /-0.7	0.7
Weight	85.4 + /-0.9	81.8 + /-1.1	0.6
Height	175.4 + /-0.3	172.6 + /-0.6	0.3
BMI	**27.6 + /-0.2**	**27.37 + /-0.3**	0.9
Diastolic Blood Pressure	79.5 + /-0.5	70.8 + /-0.8	0.04
Systolic Blood pressure	135.6 + /-0.6	127.8 + /-0.9	0.1
Heart Rate	70.0 + /-0.4	72.2 + /-0.7	0.5
Smoking History	11.5 + /-0.5	16.9 + /-1.7	0.4

3.2. Inter and intra observer variability

There were 48 replicate vascuCAP calculations made by each of the two readers on 48 coronary arteries (LM. LAD, LCx and RCA) from 14 subjects. In Table 2, the results of inter- and intra-reader variability are outlined. All measurements at .5 mm spacing were included. In general, inter-reader wSDs were slightly higher than the intra-reader wSDs. Variability in the semi-automated software were well within the range of previous variability reported on manual analysis.

3.3. Risk prediction

Clinical risk factors, both binary and continuous, were used in univariate analysis to determine the prognostic value of each individual factor, Table 3. None of the risk factors showed statistically significant prognostic value. Fig. 1 shows the scaled heat maps, indicating relationships after unsupervised hierarchical clustering of risk factors for each patient. Hypercholesterolemia and hypertension, as well as race and diabetes history, were the most closely related risk factors. Systolic blood pressure was least related to any other risk factor.

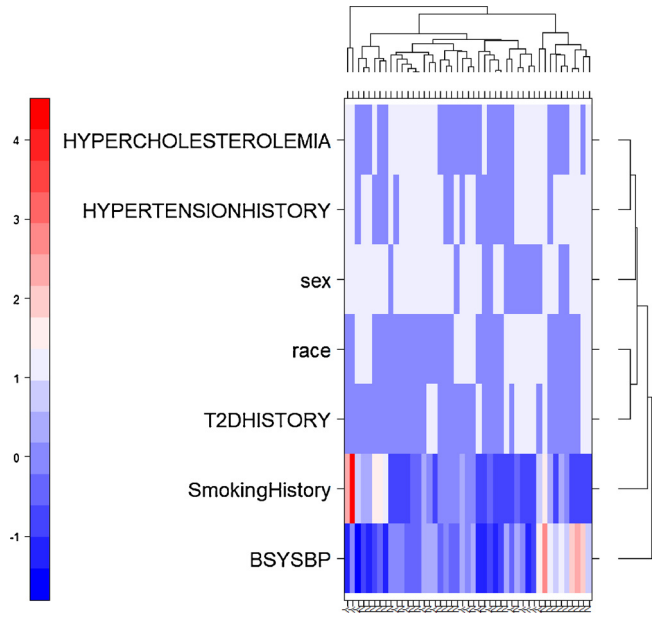

Fig. 1. Heat map indicating relationships after unsupervised hierarchical clustering of risk factors selected for the model, by patient. Hypercholesterolemia and hypertension, as well as race and diabetes history, are the most closely related risk factors. Systolic blood was least related to any other risk factor. Risk factors are centered and scaled.

Discriminatory power on a univariate basis of quantitative morphology markers calculated by the software prototype for predicting MACE was assessed. Minimum cap thickness, lesion length, LRNC volume and cross-sectional area, remodeling ratio, and wall area/thickness had high levels of predictive power, whereas calcification had equivocal predictive power (Table 4, Fig. 2). Fig. 3 shows the heat map indicating relationships after unsupervised hierarchical clustering of plaque morphology measurements for each patient. Maximum wall thickness and remodeling ratio, as well as maximum cross-sectional wall area and lesion length, are the most closely related morphology predictors. Cap thickness (smallest distance from LRNC to lumen) was least related to any other risk factor. CCTA plaque morphology resulted in a net reclassification improvement of 59% using logistic regression models and 70% using tree-based models relative to conventional risk factors.

3.4. Diagnostic accuracy

Regression analysis using clinical risk factors only resulted in a prognostic accuracy of 63% with a corresponding AUC of 0.587. Based on our RFE analysis, minimal cap thickness, lesion length, LRNC volume, maximal wall area/thickness, the remodeling ratio, and the calcium volume were included into our prognostic model as parameters. The use of morphologic features alone resulted in an increased accuracy of 77% with an AUC of 0.94. Combining both clinical risk factors and morphological features in a multivariate logistic regression analysis increased the accuracy to 87% with a similar AUC of 0.924. An overview of accuracy and ROC curves are given in Fig. 4.

Fig. 5A shows a MACE positive patient where CCTA indicates extensive plaque burden and a very long lesion, both calcified (yellow) and non-calcified (green). Fig. 5B shows a patient with a plaque with a lipid rich necrotic core (yellow) and relatively thin cap (matrix is shown in blue). The software suggested this patients was at high risk for MACE (78%), however, no MACE was recorded over the 12 months of follow-up. This patient may still have benefited from intensive medical therapy, as the thin cap would still be considered dangerous. Thus the 12 month follow-up may perhaps have been too short in this case.

4. Discussion

This study evaluates a model-based algorithm for the determination of quantitative plaque characteristics and the prognostic value for MACE, compared to, and in combination with, clinical risk factors. The results of our study demonstrate that CCTA-derived quantitative morphological features show discriminatory power to predict future cardiac events and significantly improve the prognostic value compared to clinical risk factors alone, increasing the accuracy from 0.629 to 0.872.

A study by Tesche et al. on the prognostic implications of plaque features in overlapping population as the current study showed similar prognostic accuracy compared to our results. This is significant because whereas the prior result was the result of highly skilled manual assessment. In this case however, the calculations were performed with software which has the benefit of being potentially more efficient in clinical workflow, and readers with less specific experience in the assessment may be able to reach the same level of performance as experts. Using a combination of clinical risk factors and morphological features (clinical risk factors, Napkin-ring sign, lesion length, and remodeling index) showed the highest predictive value for MACE with an of AUC 0.92. This is comparable with the AUC results in our study for the combination of risk factors and morphological features (0.924) [11].

Calcium volume was the most equivocal parameter included in our prognostic morphology model, whereas previous studies show that calcium scoring is a strong predictor of events, especially in the absence of CTA information [13–15]. The presence of calcium shows a strong correlation with the presence and extent of plaque in general. It is

Table 4
Morphology feature summary statistics.

Morphology	Negative MACE (n = 29)	Positive MACE (n = 16)	log noMACE	log MACE	PValue
Minimum CAP thickness (μm)	633.47	128.25	2.8 + /-0.019	2.11 + /-0.026	0.000
Lesion Length (μm)	0.13	27.9	−0.89 + /-0.074	1.45 + /-0.013	0.000
LRNC Volume (μm ^{3})	0.08	20.9	−1.11 + /-0.072	1.32 + /-0.04	0.000
LRNC Volume Proportion (fraction)	0.01	0.08	−2.1 + /-0.035	−1.11 + /-0.036	0.000
Max LRNC Area (μm ^{2})	0.04	3.65	−1.38 + /-0.062	0.56 + /-0.03	0.000
Max LRNC Area Proportion (fraction)	0.01	0.27	−1.9 + /-0.042	−0.57 + /-0.015	0.000
Max Wall Area (μm ^{2})	0.15	20.95	−0.83 + /-0.076	1.32 + /-0.025	0.000
Max Wall Thickness (μm)	0.05	2.21	−1.27 + /-0.061	0.34 + /-0.009	0.000
Plaque Burden Volume Ratio (unitless)	0.03	0.55	−1.55 + /-0.051	−0.26 + /-0.008	0.000
Wall Volume (μm ^{3})	0.4	248.81	−0.39 + /-0.092	2.4 + /-0.021	0.000
Max Remodeling Ratio (unitless)	1.59	3.83	0.2 + /-0.01	0.58 + /-0.024	0.001
CALC Volume (μm ^{3})	0.16	4.38	−0.79 + /-0.078	0.64 + /-0.125	0.026
Max Stenosis By Area (%)	0.01	0.08	−2.08 + /-0.047	−1.12 + /-0.088	0.026
Max CALC Area (μm ^{2})	0.08	1.09	−1.12 + /-0.066	0.04 + /-0.102	0.031
Max CALC Area Proportion (%)	0.02	0.12	−1.66 + /-0.047	−0.91 + /-0.07	0.044
CALC Volume Proportion (fraction)	0.01	0.04	−1.85 + /-0.041	−1.37 + /-0.058	0.127

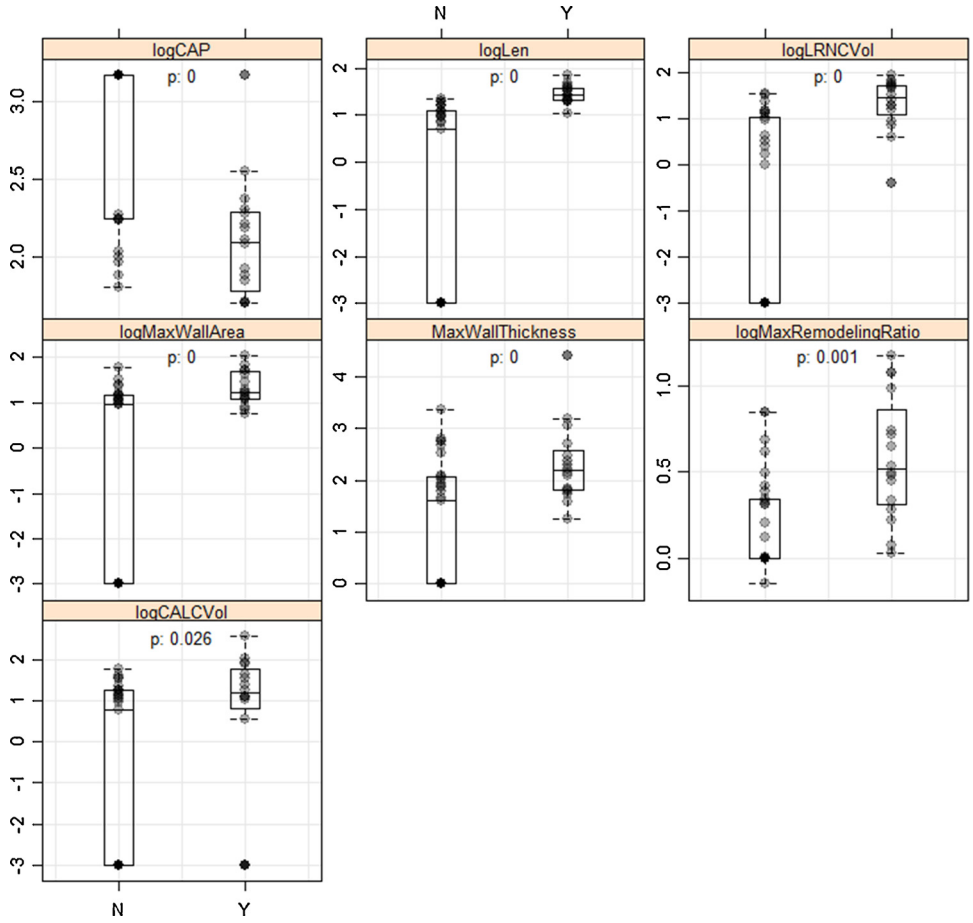

Fig. 2. Univariate box plots on logarithmic scale for vascuCAP-calculated morphology measurements. N = Negative MACE group, Y = Positive MACE group. CAP = minimum distance from LRNC to lumen, Len = lesion length, LRCNCVol = lipid-rich necrotic core volume, CALCVol = Calcium Volume.

suggested that this correlation is what plays an important role in the prognostication of MACE, not simply the presence of calcium alone. Tesche et al. found that calcified plaque volume did not significantly contribute to the prognostication of MACE and this parameter was not taken into account in their prognostic model [11]. While our model did include calcium volume, this was the least significant parameter and had limited added value. Calcification was not found to be significantly associated with MACE in univariate analyses. This is consistent with data suggesting that calcium is often a feature of older plaques and does not necessarily imply a high-risk phenotype. It may actually provide some degree of mechanical stability to a plaque surface. It is interesting to note, however, that upon performing logistic regression analysis, calcium as well as LRNC were both associated with MACE. Although calcium is often a feature of relatively stable plaques, these results raise the concern that the coexistence of LNRC with other high-risk plaque elements may signify endothelial dysfunction, ultimately stabilizing calcium but through a more dangerous intermediate development period [16]. Nance et al. found the following hazard ratios by analyzing the data of 458 patients that presented to the emergency room with acute chest pain: 57.6 for non-calcified plaques, 55.8 for partially

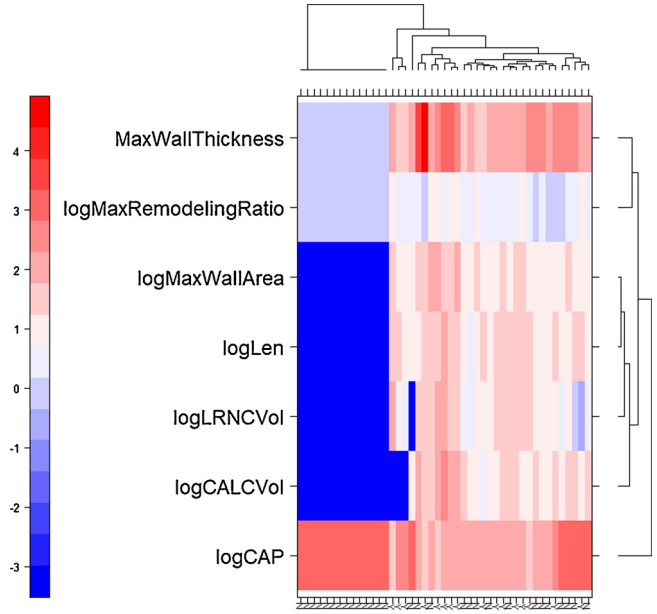

Fig. 3. Heat map indicating relationships after unsupervised hierarchical clustering of plaque morphology measurements selected by the model, by patient. Maximum wall thickness and remodeling ratio, as well as maximum cross-sectional wall area and lesion length, are the most closely related risk factors. Cap thickness (smallest distance from LRNC to lumen) was least related to any other risk factor. Risk factors are centered and scaled. The large blue block on the left are those patients for which disease was diffuse rather than forming a focal lesion.

calcified plaques, and 26.5 for solely calcified plaques. These hazard ratios indicate that calcified plaque results in a lower risk of MACE than non-calcified plaque [17]. Similarly, Bauer et al. showed that non-calcified plaque burden is a better predictor of myocardial ischemia at stress myocardial perfusion imaging than both calcium score and degree of stenosis [8].

Other morphological features that showed high prognostic value and were taken into account for prognostication in this study were cap thickness, lesion length, LRNC volume, wall area/ thickness, and remodeling ratio. Previous studies by Dey et al. showed that lesion length and LLRNC volume was higher in patients with ACS and showed significant prognostic value for the prediction of MACE [4,11]. This finding is confirmed by this study, where lesion length, LRNC volume, and remodeling index were major contributors to the prognostication of MACE. In a secondary analysis of the PROMISE trial on 4415 patients, Ferencik et al. found that high risk plaques, determined by features similar to those used in this study (i.e. remodeling ratio, low attenuation, and napkin ring sign), resulted in an increased hazard ratio of 2.73 [10]. Similarly, Nadjiri et al. found that low attenuation plaque, plaque burden, remodeling ratio, and presence of the napkin-ring sign are predictors of MACE independent of clinical risk presentation [6].

Whereas most studies on plaque morphology use visual assessment or threshold based classification, our study included a model based quantification algorithm. This approach allowed us to avoid using pre-specified thresholds for generalization over different scanners and scan protocols as well as take into account differences in contrast intensity and inter-patient characteristics, while reducing observer variability by eliminating the option to manually adjust thresholds. Key limitations of threshold based approaches include the following: partial volume effects that obscure the true interfaces of heterogeneous tissue and unmitigated lumen, the outer walls are not segmented well or are even just estimated with a fixed-radius away from the lumen constant, and tissue characteristics are determined by HU range. Limited by the above points and exacerbated by scanner variability [17], users of the threshold approach are generally encouraged to edit the ranges that create an arbitrary result that then lacks objective histological validation.

An important question is the extent to which use of coronary tissue is required for histological validation. The software used in this study utilized endarterectomy specimens collected from the carotids instead of coronaries. However, plaque characteristics such as a large atheromatous core with lipid-rich content, a thin fibrous cap, remodeling ratio greater than 1, infiltration of the plaque with macrophages and lymphocytes, and thinning of the media are predisposing to vulnerability and rupture. These plaque characteristics are similar in both carotid and coronary artery disease [18]. Plaque composition is similar in coronary and carotid arteries, irrespective of its age, and this will largely determine relative stability [19]. This suggests a similar presentation at both coronary and carotid CTA. Minor differences in the extent of the various plaque features may include a thicker fibrous cap, a higher prevalence of intraplaque hemorrhage (IPH), and calcified nodules in the carotid arteries. However, there is no difference in the nature of plaque components [18]. In addition, the carotid and coronary arteries have many similarities in the physiology of vascular tone regulation which has effects on plaque evolution [20]. Myocardial

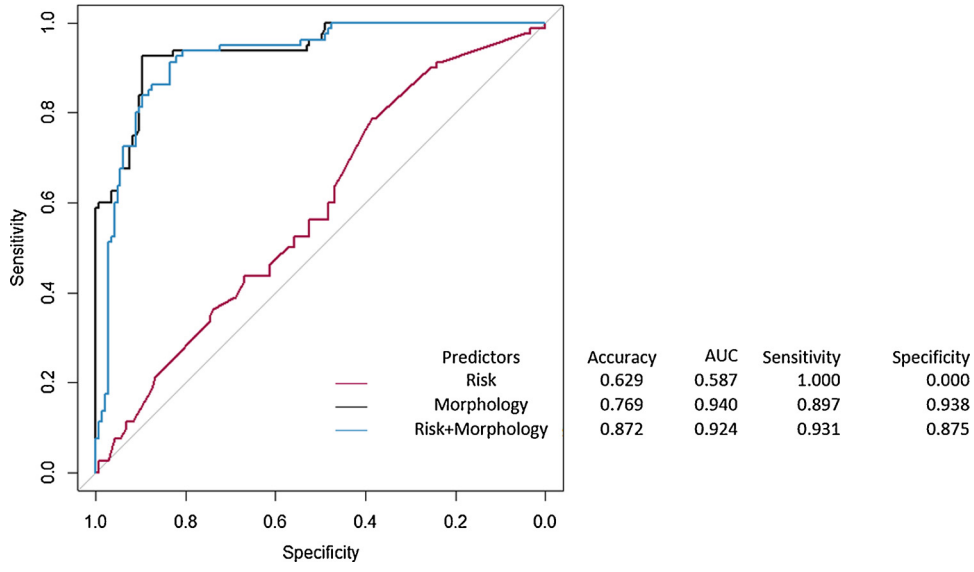

Fig. 4. ROC analysis of morphology vs. risk factors with corresponding AUCs.

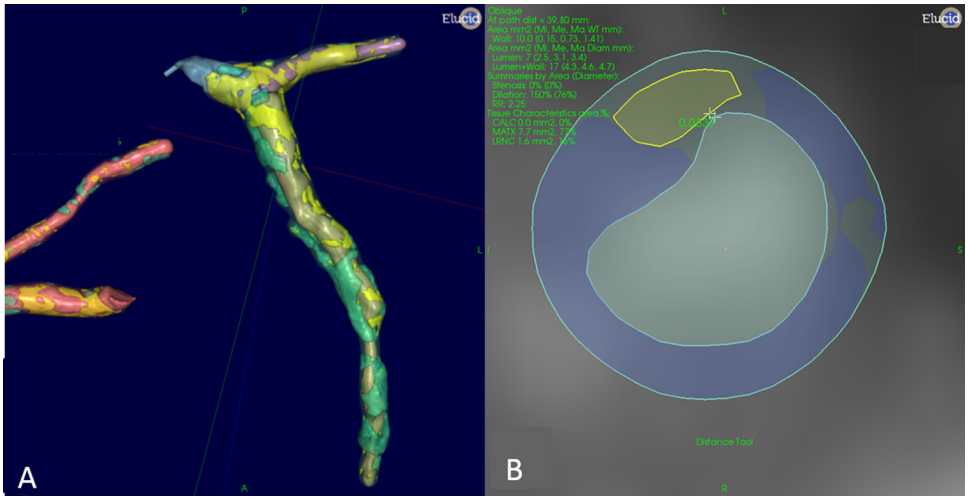

Fig. 5. Examples of plaque morphology in two patients. Panel A shows a case where the model correctly predicted MACE, and panel B shows a case where the model predicted MACE but no MACE was recorded.

blood perfusion is regulated by the vasodilation of epicardial coronary arteries in response to a variety of stimuli such as nitric oxide, causing dynamic changes in coronary arterial tone that can lead to multifold changes in coronary blood flow. In a similar fashion, carotid arteries are more than simple conduits supporting the brain circulation. They demonstrate vasoactive properties in response to stimuli, including shear stress changes [21]. Endothelial shear stress contributes to endothelial health and a favorable vascular wall transcriptomic profile [22]. Clinical studies have demonstrated that areas of low endothelial shear stress in the coronary tree are associated with atherosclerosis development and high-risk plaque features [23]. Similarly, in the carotid arteries, lower wall shear stress is associated with plaque development and localization [24].

A recent parameter, CT derived fractional flow reserve (FFR), can be considered a complementary measure, where studies increasingly show that morphology can predict FFR but not the converse. Morphological features could complement CT-FFR measurements by measuring the structural changes that precede functional deficits. The combination of plaque morphology and degree of luminal stenosis may explain outcomes in lesions with both normal and abnormal FFR [25,26]. Lesions with a large necrotic core may develop dynamic stenosis [26] due to outward remodeling during plaque formation resulting in more tissue to stretch, the tissue being stiffer, or the smooth muscle layer being already stretched to the limits of Glagov phenomenon, after which the lesions encroach on the lumen itself [27]. Likewise, inflammatory insult and/or oxidative stress could result in local endothelial dysfunction [28–31].

Clinical guidelines regarding the optimal management of patients with differing assessments of flow reserve are increasingly available [26,28,32]. Whereas it is reported that assessment of plaque morphology with high-risk features (e.g., large necrotic core and thin cap) which portend a maximum likelihood of future events may be predictive of flow reserve [33–35], but importantly, not all lesions with FFR $<$ .8 have a high likelihood of future events [33,36–38].

Without accurate assessments of plaque morphology, approaches to determine FFR using computational fluid dynamics (CFD) have been published, but CFD-based flow reserve considers only the lumen. Using only the luminal information eliminates the ability to anticipate what can occur if stress in fact causes rupture. Rather, characterizing the tissue solves these problems. The importance of providing accurate assessment by morphology is strengthened by the studies that increasingly show that morphology can predict FFR but not the converse [39,40]. That is, effectively assessed morphology may be used to calculate FFR and can also determine discontinuous changes in the plaque that move the patient from ischemia to infarction.

This study has several limitations that deserve mention. We present a retrospective case-controlled study investigation with a limited follow-up time, which is therefore subject to limitations inherent to this type of study design. A relatively small number of patients were included, which may incur selection bias. Therefore, prospective studies on larger study cohorts will be necessary to validate our findings. This study used multiple CT systems, which could introduce variability, on the other hand it shows that the value of model based analysis independent of CT system used. Further studies are needed to investigate the role of variability caused by different CT systems. Additionally, although the software used in this study also has an experimental capability for measurements of IPH, we did not enable that capability in this study. However, it could prove useful given the clinical significance attributed to IPH.

In conclusion, an automated model based algorithm to evaluate CTA-derived plaque features and quantify morphological features of atherosclerotic plaque increases the ability for MACE prognostication significantly compared to the use of clinical risk factors alone, while also having the potential to reduce observer variability and the time to evaluate patients relative to expert assessment.

Disclosures

Dr. Schoepf receives institutional research support and / or personal fees from Astellas, Bayer, Bracco, Elucid Bioimaging, Guerbet, HeartFlow, and Siemens. Dr. Varga-Szemes receives institutional research support and / or personal fees from Elucid Bioimaging, Guerbet and Siemens. UMCG receives institutional research support from Siemens. Elucid Bioimaging authors are employed by a company that commercializes plaque morphology assessment software. The other authors have no conflict of interest to disclose.

Appendix A. Supplementary data

Supplementary material related to this article can be found, in the online version, at doi:https://doi.org/10.1016/j.ejrad.2019.04.013.

References

[1] W.B. Meijboom, M.F.L. Meijs, J.D. Schuijf, et al., Diagnostic accuracy of 64-Slice computed tomography coronary angiography. A prospective, multicenter, multivendor study, J. Am. Coll. Cardiol. 52 (25) (2008) 2135–2144, https://doi.org/10.1016/j.jacc.2008.08.058.
[2] M.M. Miller, C.A. Ridge, D.E. Litmanovich, Computed tomography angiographic

assessment of acute chest pain, J. Thorac. Imaging 32 (3) (2017) 137–150, https://doi.org/10.1097/RTI.0000000000000267.
[3] J.K. Min, J. Feignoux, J. Treutenaere, T. Laperche, J. Sablayrolles, The prognostic value of multidetector coronary CT angiography for the prediction of major adverse cardiovascular events: a multicenter observational cohort study, Int. J. Cardiovasc. Imaging 26 (6) (2010) 721–728, https://doi.org/10.1007/s10554-010-9613-4.
[4] D. Dey, S. Achenbach, A. Schuhbaeck, et al., Comparison of quantitative atherosclerotic plaque burden from coronary CT angiography in patients with first acute coronary syndrome and stable coronary artery disease, J. Cardiovasc. Comput. Tomogr. 8 (5) (2014) 368–374, https://doi.org/10.1016/j.jcct.2014.07.007.
[5] B.M. Ohnesorge, L.K. Hofmann, T.G. Flohr, U.J. Schoepf, CT for imaging coronary artery disease: defining the paradigm for its application, Int. J. Cardiovasc. Imaging 21 (1) (2005) 85–104, https://doi.org/10.1007/s10554-004-5346-6.
[6] J. Nadjiri, J. Hausleiter, C. Jähnichen, et al., Incremental prognostic value of quantitative plaque assessment in coronary CT angiography during 5 years of follow up, J. Cardiovasc. Comput. Tomogr. 10 (2) (2016) 97–104, https://doi.org/10.1016/j.jcct.2016.01.007.
[7] S. Baumann, P. Kryeziu, C. Tesche, et al., Association of serum lipid profile with coronary computed tomographic angiography-derived morphologic and functional quantitative plaque markers, J. Thorac. Imaging (2018).
[8] R.W. Bauer, C. Thilo, S.A. Chiaramida, T.J. Vogl, P. Costello, U.J. Schoepf, Noncalcified atherosclerotic plaque burden at coronary CT angiography: a better predictor of ischemia at stress myocardial perfusion imaging than calcium score and stenosis severity, Am. J. Roentgenol. 193 (2) (2009) 410–418, https://doi.org/10.2214/AJR.08.1277.
[9] M.S. Bittencourt, E. Hulten, B. Ghoshhajra, et al., Prognostic value of nonobstructive and obstructive coronary artery disease detected by coronary computed tomography angiography to identify cardiovascular events, Circ. Cardiovasc. Imaging 7 (2) (2014) 282–291, https://doi.org/10.1161/CIRCIMAGING.113.001047.
[10] M. Ferencik, T. Mayrhofer, D.O. Bittner, et al., Use of high-risk coronary atherosclerotic plaque detection for risk stratification of patients with stable chest pain: a secondary analysis of the promise randomized clinical trial, JAMA Cardiol. 3 (2) (2018) 144–152, https://doi.org/10.1001/jamacardio.2017.4973.
[11] C. Tesche, F. Plank, C.N. De Cecco, et al., Prognostic implications of coronary CT angiography-derived quantitative markers for the prediction of major adverse cardiac events, J. Cardiovasc. Comput. Tomogr. 10 (6) (2016) 458–465, https://doi.org/10.1016/j.jcct.2016.08.003.
[12] M. Sheahan, X. Ma, D. Paik, et al., Atherosclerotic plaque tissue: noninvasive quantitative assessment of characteristics with software-aided measurements from conventional CT angiography, Radiology 000 (0) (2017) 170127, , https://doi.org/10.1148/radiol.2017170127.
[13] A.A. Kelkar, W.M. Schultz, F. Khosa, et al., Long-term prognosis after coronary artery calcium scoring among low-intermediate risk women and men, Circ. Cardiovasc. Imaging 9 (4) (2016) 1–7, https://doi.org/10.1161/CIRCIMAGING.115.003742.
[14] H.S. Hecht, Coronary artery calcium scanning: past, present, and future, JACC Cardiovasc. Imaging 8 (5) (2015) 579–596, https://doi.org/10.1016/j.jcmg.2015.02.006.
[15] J. Yeboah, R.L. McClelland, T.S. Polonsky, et al., Comparison of novel risk markers for improvement in cardiovascular risk assessment in intermediate-risk individuals, JAMA 308 (8) (2012) 788, https://doi.org/10.1001/jama.2012.9624.
[16] M. Kuhn, K. Johnson, Applied Predictive Modeling, (2017).
[17] J.W. Nance, C.L. Schlett, U.J. Schoepf, et al., Incremental prognostic value of different components of coronary atherosclerotic plaque at cardiac CT angiography beyond coronary calcification in patients with acute chest pain, Radiology 264 (3) (2012) 679–690, https://doi.org/10.1148/radiol.12112350.
[18] J.A. Schaar, J.E. Muller, E. Falk, et al., Terminology for high-risk and vulnerable coronary artery plaques, Eur. Heart J. 25 (12) (2004) 1077–1082, https://doi.org/10.1016/j.ehj.2004.01.002.
[19] P. Ibrahimi, F. Jashari, R. Nicoll, G. Bajraktari, P. Wester, M.Y. Henein, Coronary and carotid atherosclerosis: how useful is the imaging? Atherosclerosis 231 (2) (2013) 323–333, https://doi.org/10.1016/j.atherosclerosis.2013.09.035.
[20] F. Sigala, E. Oikonomou, A.S. Antonopoulos, G. Galyfos, D. Tousoulis, Coronary versus carotid artery plaques. Similarities and differences regarding biomarkers morphology and prognosis, Curr. Opin. Pharmacol. 39 (Figure 1) (2018) 9–18, https://doi.org/10.1016/j.coph.2017.11.010.
[21] H.H. Carter, C.L. Atkinson, I.H.A. Heinonen, et al., Evidence for shear stress-mediated dilation of the internal carotid artery in humans, Hypertension 68 (5) (2016) 1217–1224, https://doi.org/10.1161/HYPERTENSIONAHA.116.07698.
[22] J.R. Davies, J.H.F. Rudd, P.L. Weissberg, J. Narula, Radionuclide imaging for the detection of inflammation in vulnerable plaques, J. Am. Coll. Cardiol. 47 (8 SUPPL) (2006), https://doi.org/10.1016/j.jacc.2005.11.049.
[23] Y.S. Chatzizisis, K. Toutouzas, A.A. Giannopoulos, et al., Association of global and local low endothelial shear stress with high-risk plaque using intracoronary 3D optical coherence tomography: introduction of' shear stress score, Eur. Heart J. Cardiovasc. Imaging 18 (8) (2017) 888–897, https://doi.org/10.1093/ehjci/jew134.
[24] A. Gnasso, C. Irace, C. Carallo, et al., In vivo association between low wall shear stress and plaque in subjects with asymmetrical carotid atherosclerosis, Stroke 28 (5) (1997) 993–998, https://doi.org/10.1161/01.STR.28.5.993.
[25] A. Ahmadi, J. Leipsic, K.A. Øvrehus, et al., Lesion-specific and vessel-related determinants of fractional flow reserve beyond coronary artery stenosis, JACC Cardiovasc. Imaging 11 (4) (2018) 521–530, https://doi.org/10.1016/j.jcmg.2017.11.020.
[26] A. Ahmadi, G.W. Stone, J. Leipsic, et al., Association of coronary stenosis and plaque morphology with fractional flow reserve and outcomes, JAMA Cardiol. 1 (3) (2016) 350–357, https://doi.org/10.1001/jamacardio.2016.0263.
[27] S. Glagov, E. Weisenberg, C.K. Zarins, Compensatory enlargement of human atherosclerotic coronary arteries, N. Engl. J. Med. 316 (22) (1987) 1371–1375, https://doi.org/10.1056/NEJM198705283162204.
[28] A. Ahmadi, A. Kini, J. Narula, Discordance between ischemia and stenosis, or PINSS and NIPSS: are we ready for new vocabulary? JACC Cardiovasc. Imaging 8 (1) (2015) 111–114, https://doi.org/10.1016/j.jcmg.2014.11.010.
[29] S. Lavi, J.H. Bae, C.S. Rihal, et al., Segmental coronary endothelial dysfunction in patients with minimal atherosclerosis is associated with necrotic core plaques, Heart 95 (18) (2009) 1525–1530, https://doi.org/10.1136/hrt.2009.166017.
[30] S. Lavi, J.P. McConnell, C.S. Rihal, et al., Local production of lipoprotein-associated phospholipase A2 and lysophosphatidylcholine in the coronary circulation: Association with early coronary atherosclerosis and endothelial dysfunction in humans, Circulation 115 (21) (2007) 2715–2721, https://doi.org/10.1161/CIRCULATIONAHA.106.671420.
[31] S. Lavi, E.H. Yang, A. Prasad, et al., The interaction between coronary endothelial dysfunction, local oxidative stress, and endogenous nitric oxide in humans, Hypertension 51 (1) (2008) 127–133, https://doi.org/10.1161/HYPERTENSIONAHA.107.099986.
[32] B.L. Nørgaard, J. Leipsic, S. Gaur, et al., Diagnostic performance of noninvasive fractional flow reserve derived from coronary computed tomography angiography in suspected coronary artery disease, J. Am. Coll. Cardiol. 63 (12) (2014) 1145–1155, https://doi.org/10.1016/j.jacc.2013.11.043.
[33] S. Motoyama, H. Ito, M. Sarai, et al., Plaque characterization by coronary computed tomography angiography and the likelihood of acute coronary events in mid-term follow-up, J. Am. Coll. Cardiol. 66 (4) (2015) 337–346, https://doi.org/10.1016/j.jacc.2015.05.069.
[34] G.W. Stone, A. Maehara, A.J. Lansky, et al., A prospective natural-history study of coronary atherosclerosis, N. Engl. J. Med. 364 (3) (2011) 226–235, https://doi.org/10.1056/NEJMoa1002358.
[35] A. Ahmadi, J. Leipsic, R. Blankstein, et al., Do plaques rapidly progress prior to myocardial infarction? The interplay between plaque vulnerability and progression, Circ. Res. 117 (1) (2015) 99–104, https://doi.org/10.1161/CIRCRESAHA.117.305637.
[36] S. Kaul, J. Narula, In search of the vulnerable plaque: is there any light at the end of the catheter? J. Am. Coll. Cardiol. 64 (23) (2014) 2519–2524, https://doi.org/10.1016/j.jacc.2014.10.017.
[37] J. Narula, M. Nakano, R. Virmani, et al., Histopathologic characteristics of atherosclerotic coronary disease and implications of the findings for the invasive and noninvasive detection of vulnerable plaques, J. Am. Coll. Cardiol. 61 (10) (2013) 1041–1051, https://doi.org/10.1016/j.jacc.2012.10.054.
[38] R.M. Oemrawsingh, J.M. Cheng, H.M. García-García, et al., Near-infrared spectroscopy predicts cardiovascular outcome in patients with coronary artery disease, J. Am. Coll. Cardiol. 64 (23) (2014) 2510–2518, https://doi.org/10.1016/j.jacc.2014.07.998.
[39] K.N. Jin, C.N. De Cecco, D. Caruso, et al., Myocardial perfusion imaging with dual energy CT, Eur. J. Radiol. 85 (10) (2016) 1914–1921, https://doi.org/10.1016/j.ejrad.2016.06.023.
[40] A. Coenen, Y.-H. Kim, M. Kruk, et al., Diagnostic accuracy of a machine-learning approach to coronary computed tomographic angiography–based fractional flow reserve, Circ. Cardiovasc. Imaging 11 (6) (2018) e007217, , https://doi.org/10.1161/CIRCIMAGING.117.007217.